


## Constraining the curvature density parameter in cosmology

Purba Mukherjee<sup>\*</sup> and Narayan Banerjee<sup>†</sup>

*Department of Physical Sciences, Indian Institute of Science Education and Research Kolkata,  
Mohanpur, West Bengal - 741246, India*

 (Received 10 October 2021; accepted 15 February 2022; published 15 March 2022)

The cosmic curvature density parameter has been constrained in the present work independent of any background cosmological model. The reconstruction is undertaken adopting the nonparametric Gaussian processes (GP). The constraints on  $\Omega_{k0}$  are obtained via a Markov Chain Monte Carlo (MCMC) analysis. Late-time cosmological probes viz., the supernova (SN) distance modulus data, the cosmic chronometer (CC) and the radial baryon acoustic oscillations (*r*BAO) measurements of the Hubble data have been utilized for this purpose. The results are further combined with the data from redshift space distortions (RSD) which studies the growth of large scale structure in the universe. The only *a priori* assumption is that the universe is homogeneous and isotropic, described by the Friedmann-Lemaître-Robertson-Walker metric. Results indicate that a spatially flat universe is well consistent in  $2\sigma$  within the domain of reconstruction  $0 < z < 2$  for the background data. On combining the RSD data we find that the results obtained are consistent with spatial flatness mostly within  $2\sigma$  and always within  $3\sigma$  in the domain of reconstruction  $0 < z < 2$ .

DOI: [10.1103/PhysRevD.105.063516](https://doi.org/10.1103/PhysRevD.105.063516)

### I. INTRODUCTION

The universe on a large scale is described by the spatially homogeneous and isotropic Friedmann-Lemaître-Robertson-Walker (FLRW) metric,

$$ds^2 = -c^2 dt^2 + a^2(t) \left[ \frac{dr^2}{1 - kr^2} + r^2 d\theta^2 + r^2 \sin^2 \theta d\phi^2 \right]. \quad (1)$$

The scale factor  $a(t)$  is the only unknown function to be determined by the field equations. The isotropy and homogeneity of the space section demand the spatial curvature to be a constant, which can thus be scaled to pick up values from  $-1, +1, 0$ . This constant spatial curvature is termed the curvature index and is denoted as  $k$ . This index is not determined by the field equations but is rather fixed by hand, essentially from observational requirements.

The effect of the spatial curvature  $k$  in the evolution of the universe is estimated through the curvature density parameter, defined as,

$$\Omega_k = -\frac{kc^2}{a^2 H^2}, \quad (2)$$

where  $H = \frac{\dot{a}}{a}$  is the Hubble parameter.  $\Omega_k$  is positive, negative or zero corresponding to  $k = -1, +1, 0$ , which in

turn correspond to open, closed, and flat space sections, respectively.

For the standard cosmological model to correctly describe the present state of the evolution, the initial value of  $\Omega_k$  has to be tantalizingly close to zero, indicating that the universe essentially starts with a zero spatial curvature. This is known as the flatness or fine-tuning problem for the standard cosmology which is believed to be taken care of by an early accelerated expansion called inflation. For a brief but systematic description, we refer to the monograph by Liddle and Lyth [1]. Indeed inflation can wash out an early effect of spatial curvature, in comparison with the inflaton energy and the Hubble expansion. However, if  $\Omega_k$  is negligible but  $k$  itself is nonzero, it may reappear in course of evolution and make its presence felt as the universe evolves. Reconstruction of some dark energy parameters indicate that a nonflat space section may not be easily ruled out. The use of  $\Omega_k$  as a free parameter is found to affect the reconstruction of dark energy equation of state parameter  $w(z)$ , as shown by Clarkson *et al.* [2]. A reconstruction of the deceleration parameter  $q(z)$  by Gong and Wang [3] shows that although a flat universe is still consistent,  $|\Omega_{k0}|$  is less than only 0.05 for a one-parameter dark energy model and lies between  $-0.064$  and  $0.028$  for a  $\Lambda$ CDM model with spatial curvature, where a subscript 0 indicates the present value of the quantity. The recent Planck [4] data also indicates that a universe with a nonzero spatial curvature may not be completely ruled out.

The motivation of the present work is to constrain the curvature density parameter  $\Omega_{k0}$  hence attempt to ascertain

<sup>\*</sup>pm14ip011@iiserkol.ac.in  
<sup>†</sup>narayan@iiserkol.ac.in

the signature of the curvature index  $k$ , directly from observational data without assuming any background cosmological model. We do not start from any theory of gravity or use any form of matter distribution in the universe. The only *a priori* assumption is that the universe is homogeneous and isotropic, and thus described by the FLRW metric. There is quite a lot of interest in this direction, which is normally pursued along with constraining other cosmological parameters pertaining to the alleged accelerated expansion of the universe. Most of these investigations depend on some chosen parametric form of cosmological quantities related to the late-time expansion behavior of the universe [5–14]. This approach is indeed biased by the parametrization, as the functional form of the quantity is already chosen.

Another way of reconstruction involves a verification of the FLRW metric from datasets, and ascertaining the value of  $\Omega_{k0}$  as a by-product by combining the dimensionless reduced Hubble parameter  $E(z)$  and the normalized comoving distance  $D(z)$  [2,15–20].

The present work does not assume any functional form of  $\Omega_k$ , but rather resorts to a nonparametric reconstruction of  $\Omega_{k0}$ , the present value of the curvature density parameter. The idea is to obtain constraints on the geometrical quantity  $\Omega_{k0}$  using recent observational data provided by the high precision cosmological probes, namely, the supernova (SN) distance modulus data, the cosmic chronometer (CC) and the radial baryon acoustic oscillations (*r*BAO) measurements of the Hubble parameter. We also combine these data from background measurements with the data from redshift space distortions (RSD) due to the growth of large scale structures. The reconstruction is performed adopting the nonparametric Gaussian processes (GP) method. The resulting marginalized constraints on  $\Omega_{k0}$  are obtained via a Markov Chain Monte Carlo (MCMC) analysis, independent of any parametric model of the expansion history.

Attempts toward obtaining constraints on  $\Omega_{k0}$  using the nonparametric approach started to gain momentum in the recent past. Li *et al.* [21], Wei and Wu [22] proposed to constrain the cosmic curvature in a model-independent way by combining the  $CC-H(z)$  with Union 2.1 [23], and Joint Light-curve Analysis (JLA) [24] SN-Ia data respectively. Model-independent constraints on cosmic curvature and opacity was carried out by Wang *et al.* [25] using the  $CC-H(z)$  and JLA SN-Ia data. Liao [26] studied constraints on cosmic curvature with lensing time delays and gravitational waves (GWs). Model-independent distance calibration and  $\Omega_{k0}$  measurement using quasistellar objects (QSOs) and CCs was done by Wei and Melia [27]. Ruan *et al.* [28] obtained constraints on  $\Omega_{k0}$  using the  $CC-H(z)$  data and HII galaxy Hubble diagram. Model-independent estimation for  $\Omega_{k0}$  from the latest strong gravitational lens systems (SGLs) was performed by Zhou and Li [29]. Wang *et al.* [30] constrained  $\Omega_{k0}$  from SGL and Pantheon [31] SN-Ia

observations. Wang *et al.* [32] employed a machine learning algorithm called artificial neural network (ANN) to constrain  $\Omega_{k0}$  using data from CC, SN-Ia and GWs. Recently, Yang and Gong [33] constrained the  $\Omega_{k0}h^2$  using  $CC-H(z)$ , Pantheon SN-Ia and RSD data where  $h = \frac{H_0}{100 \text{ km Mpc}^{-1} \text{ s}^{-1}}$  is the dimensionless Hubble parameter at the present epoch. Nonparametric spatial curvature inference using CC and Pantheon data was performed by Dhawan *et al.* [34]. A majority of these investigations use GP as their numerical tool.

We use observational data more recent than most of these investigations, but the major difference is that we include a wider variety of data in combination, measuring different features of the evolution. We also include a section where the RSD dataset which has mostly eluded the attention so far, except the work of Yang and Gong [33] in the reconstruction of  $\Omega_{k0}h^2$  despite its utmost relevance in this connection, as the growth of perturbations has to be consistent with the spatial curvature.

The other crucial addition in the present work is that we also check the consistency of the constraints on spatial curvature with thermodynamic requirements. Very recently, Ferreira and Pavón [35] imposed a relation using the generalized second law of thermodynamics, which reads as  $1 + q \geq \Omega_k$ , where  $q$  is the deceleration parameter. It is quite reassuring to see that constraints on  $\Omega_{k0}$  quite comfortably satisfies the requirement.

The results obtained indicate that a spatial curvature may indeed exist at the present epoch. But the estimated sign of the curvature depends on the strategies for measuring  $H_0$  to some extent. But the results are statistically not too significant, as a zero curvature is mostly included in  $1\sigma$  and always at least in  $2\sigma$ .

The paper is organized as follows. Section II contains the details on the reconstruction method. In Sec. III, the observational data used in the present work have been briefly reviewed. The methodology is discussed in Sec. IV. Reconstruction using background data is performed in Sec. V. Section VI shows the consistency of  $\Omega_{k0}$  constraints with the second law of thermodynamics. Reconstruction using the perturbation data are presented in Sec. VII. The final Sec. VIII contains an overall discussion on the results.

## II. GAUSSIAN PROCESS

We shall employ the well-known Gaussian processes (GP) [36–38] for the reconstruction of  $\Omega_{k0}$ . Assuming that the observational data obey a Gaussian distribution with mean and variance, the posterior distribution of the reconstructed function (say  $f$ ) and its derivatives can be expressed as a joint Gaussian distribution. In this method, the covariance function  $\kappa(z, \tilde{z})$  plays a key role. It correlates the values of  $f(z)$  at two redshift points  $z$  and  $\tilde{z}$ . This covariance function depends on a set of *hyperparameters* which are optimized by maximizing the log marginal

likelihood. With the optimized covariance function, the data can be extended to any redshift point. The GP method has been widely applied in cosmology [39–59].

It deserves mention that the choice of  $\kappa(z, \tilde{z})$ , affects the reconstruction to some extent. The more commonly used covariance function is the squared exponential covariance, which is infinitely differentiable,

$$\kappa(z, \tilde{z}) = \sigma_f^2 \exp\left(-\frac{(z - \tilde{z})^2}{2l^2}\right). \quad (3)$$

In this particular work we consider the squared exponential, Matérn 9/2, Cauchy and rational quadratic covariance functions. The Matérn 9/2 covariance function is given by,

$$\kappa(z, \tilde{z}) = \sigma_f^2 \exp\left(\frac{-3|z - \tilde{z}|}{l}\right) \left[1 + \frac{3|z - \tilde{z}|}{l} + \frac{27(z - \tilde{z})^2}{7l^2} + \frac{18|z - \tilde{z}|^3}{7l^3} + \frac{27(z - \tilde{z})^4}{35l^4}\right]. \quad (4)$$

The Cauchy covariance function is

$$\kappa(z, \tilde{z}) = \sigma_f^2 \left[\frac{l}{(z - \tilde{z})^2 + l^2}\right], \quad (5)$$

and the rational quadratic covariance function is

$$\kappa(z, \tilde{z}) = \sigma_f^2 \left[1 + \frac{(z - \tilde{z})^2}{2\alpha l^2}\right]^{-\alpha}, \quad (6)$$

where  $\sigma_f$ ,  $l$ , and  $\alpha$  are the kernel hyperparameters. Throughout this work, we assume a zero mean function *a priori* to characterize the GP.

For more details on the GP method, one can refer to the Gaussian process website<sup>1</sup> The publicly available GAPP<sup>2</sup> (Gaussian processes in python) code by Seikel *et al.* [40] has been used in this work.

### III. OBSERVATIONAL DATA

In this work we use both the background data and the perturbation data for the reconstruction of  $\Omega_{k0}$ . The background level includes different combinations of datasets involving the cosmic chronometer data (CC), the supernova distance modulus data (SN), the baryon acoustic oscillation data (BAO). For the perturbation level data, the growth rate of structure  $f\sigma_8$  from the redshift-space distortions (RSD) are utilized. A brief summary of the datasets is given below.

#### A. Background level

The Hubble parameter  $H(z)$  can be directly obtained from the differential redshift time derived by calculating the spectroscopic differential ages of passively evolving galaxies, usually called the cosmic chronometer (CC) method [60]. In this work we use the latest 31 CC  $H(z)$  data [61–67], covering the redshift range up to  $z \sim 2$ . These measurements do not assume any particular cosmological model.

We take into account the updated and corrected Pantheon compilation by Steinhardt *et al.* [68]. This corrected sample improves upon some errors in the quoted values of the redshift  $z$  in the original Pantheon dataset by Scolnic *et al.* [31]. The Pantheon catalogue is presently the largest spectroscopically confirmed SNIa sample, consisting of 1048 supernovae from different surveys covering the redshift range up to  $z \sim 2.3$ , including the SDSS, SNLS, various low- $z$  and some high- $z$  samples from the HST.

An alternative compilation of the Hubble  $H(z)$  data can be deduced from the radial BAO peaks in the galaxy power spectrum, or from the BAO peak using the Ly- $\alpha$  forest of quasars, which are based on the clustering of galaxies or quasi stellar objects (namely  $r$ BAO), spanning the redshift range  $0 < z < 2.4$  reported in various surveys [69–81]. One may find that some of the  $H(z)$  data points from clustering measurements are correlated since they either belong to the same analysis or there is an overlap between the galaxy samples. Here in this paper, we mainly consider the central value and standard deviation of the data into consideration. Therefore, we assume that they are independent measurements as in [56,82].

In view of the known tussle between the value of  $H_0$  as given by the Planck [4] 2018 data from the CMB measurements (hereafter referred to as P18), and that from HST observations of 70 long-period Cepheids in the Large Magellanic Clouds by the SHOES [83] team (hereafter referred to as R19), reconstruction using both of them have been carried out separately. The recent global P18 and local R19 measurements of  $H_0 = 67.27 \pm 0.60 \text{ km s}^{-1} \text{ Mpc}^{-1}$  for TT + TE + EE + lowE (P18) [4] and  $H_0 = 74.03 \pm 1.42 \text{ km s}^{-1} \text{ Mpc}^{-1}$  (R19) [83] respectively, with a 4.4 $\sigma$  tension between them, are considered for the purpose.

#### B. Perturbation level

The redshift space distortion (RSD) data is a very promising probe to distinguish between different cosmological models. Various dark energy models may lead to a similar evolution in the large scale but can show a distinguishable growth of the cosmic structure. In this work, we utilize the updated datasets of the  $f\sigma_8$  measurements, including the collected data from 2006–2018 [84–88], and the completed SDSS, extended BOSS Survey, DES and other galaxy surveys [89–109]. We refer to [82] for a recent compilation of the 63 RSD data within the redshift

<sup>1</sup><http://www.gaussianprocess.org>.

<sup>2</sup><https://github.com/carlosandrepae/GaPP>.

range  $0 < z < 2$  respectively. This  $f\sigma_8$  is called the growth rate of structure.

#### IV. THE CURVATURE DENSITY PARAMETER AND DISTANCE MEASURES

In a FLRW universe, the proper distance from the observer to a celestial object at redshift  $z$  along the line of sight is given by,

$$d_p(z) = \frac{c}{H_0} \int_0^z \frac{dz'}{E(z')} \quad (7)$$

and the transverse comoving distance can be expressed as,

$$d_M(z) = \frac{c}{H_0 \sqrt{|\Omega_{k0}|}} \sin n \left( \sqrt{|\Omega_{k0}|} \int_0^z \frac{dz'}{E(z')} \right), \quad (8)$$

in which the  $\sin n$  function is a shorthand for,

$$\sin nx = \begin{cases} \sinh x & (\Omega_{k0} > 0), \\ x & (\Omega_{k0} \rightarrow 0), \\ \sin x & (\Omega_{k0} < 0). \end{cases}$$

We define the reduced Hubble parameter as,

$$E(z) = \frac{H(z)}{H_0}. \quad (9)$$

Here, a suffix 0 indicates the value of the relevant quantity at the present epoch and  $z$  is the redshift, defined as  $1+z \equiv \frac{a}{a_0}$ . The dimensionless parameter  $\Omega_{k0}$ , namely the cosmic curvature density parameter, defined as

$$\Omega_{k0} = -\frac{kc^2}{a_0^2 H_0^2}, \quad (10)$$

is positive, negative, or zero corresponding to the spatial curvature  $k = -1, +1, 0$  which signifies an open, closed, or flat universe, respectively.

For convenience, we can define the normalized proper distance,

$$D_p(z) \equiv \frac{H_0}{c} d_p(z) \quad (11)$$

and the normalized transverse comoving distance,

$$D(z) \equiv \frac{H_0}{c} d_M(z) \quad (12)$$

as dimensionless cosmological distance measures which will be used later in our work.

#### V. RECONSTRUCTION FROM BACKGROUND DATA

In the very beginning we use the GP method to reconstruct the Hubble parameter  $H(z)$  from the CC data and CC +  $r$ BAO data. We then normalize the datasets with the reconstructed value of  $H_0$ , i.e.,  $H(z=0)$  to obtain the dimensionless or reduced Hubble parameter  $E(z)$ . Considering the error associated with the Hubble data as  $\sigma_H$ , we calculate the uncertainty in  $E(z)$  as,

$$\sigma_E = \sqrt{\frac{\sigma_H^2}{H_0^2} + \frac{H^2}{H_0^4} \sigma_{H_0}^2}, \quad (13)$$

where  $\sigma_{H_0}$  is the error associated with  $H_0$ .

With the function  $E(z)$  reconstructed from the Hubble data, as described in Eq. (9), the normalized proper distance  $D_p$  is calculated via a numerical integration using the composite trapezoidal [110] rule.

$$D_p(z) = \int_0^z \frac{dz'}{E(z')} \simeq \frac{1}{2} \sum_i (z_{i+1} - z_i) \left[ \frac{1}{E(z_{i+1})} + \frac{1}{E(z_i)} \right]. \quad (14)$$

Thus we get  $D_p$  without assuming any prior fiducial cosmological model. The error associated with  $D_p$ , say  $\sigma_{D_p}$ , is obtained from the reconstructed function  $E(z)$  along with its associated error uncertainties  $\sigma_E(z)$  described in Eq. (13), and is given by,

$$\sigma_{D_p}^2(z) \simeq \frac{1}{4} \sum_i (z_{i+1} - z_i)^2 \left[ \frac{\sigma_{E_{i+1}}^2}{E_{i+1}^4} + \frac{\sigma_{E_i}^2}{E_i^4} \right]. \quad (15)$$

From this reconstructed  $D_p$ , we can calculate the normalized transverse comoving distance  $D$  from the Hubble data as,

$$D(z) = \begin{cases} \frac{1}{\sqrt{\Omega_{k0}}} \sinh [\sqrt{\Omega_{k0}} D_p(z)] & \Omega_{k0} > 0, \\ D_p(z) & \Omega_{k0} = 0, \\ \frac{1}{\sqrt{-\Omega_{k0}}} \sin [\sqrt{-\Omega_{k0}} D_p(z)] & \Omega_{k0} < 0. \end{cases} \quad (16)$$

The error  $\sigma_D$  of the reconstructed  $D$  from the Hubble data is,

$$\sigma_D(z) = \begin{cases} \cosh [\sqrt{\Omega_{k0}} D_p(z)] \sigma_{D_p}(z) & \Omega_{k0} > 0, \\ \sigma_{D_p}(z) & \Omega_{k0} = 0, \\ \cos [\sqrt{-\Omega_{k0}} D_p(z)] \sigma_{D_p}(z) & \Omega_{k0} < 0. \end{cases} \quad (17)$$

Steinhardt *et al.* [68] lists the corrected distance modulus  $\mu$  corresponding to different redshift  $z$ , along with their



respective error uncertainties, from supernovae observations following the BEAMS with bias corrections (BBC) [111] framework.

The total uncertainty matrix of observed distance modulus given by,

$$\mathbf{\Sigma}_\mu = \mathbf{C}_{\text{stat}} + \mathbf{C}_{\text{sys}}, \quad (18)$$

where both the statistical covariance matrix  $\mathbf{C}_{\text{stat}}$  and the systematic errors  $\mathbf{C}_{\text{sys}}$  are included in our calculation.

With another Gaussian process on the observed distance modulus of the SN-Ia data, we reconstruct  $\mu_{\text{SN}}$  and the associated error uncertainties  $\sigma_{\mu_{\text{SN}}}$ , at the same redshift as that of the Hubble data. The subscript SN stands for supernova.

The distance modulus is theoretically given by,

$$\mu = 5 \log_{10} \left( \frac{d_L}{\text{Mpc}} \right) + 25. \quad (19)$$

Here,  $d_L$  is the luminosity distance. This  $d_L$  is related to the normalized transverse comoving distance  $D$  as,

$$d_L(z) = d_M(1+z) = \frac{c(1+z)D}{H_0}. \quad (20)$$

Substituting Eq. (16) in Eq. (19), we estimate the reconstructed distance modulus from the Hubble data, say  $\mu_H$  along with its  $1\sigma$  error uncertainty  $\sigma_{\mu_H}$  as,

$$\mu_H = 5 \log_{10} \left[ \frac{c(1+z)D}{H_0} \right] + 25, \quad (21)$$

$$\sigma_{\mu_H} = \frac{5}{\ln 10} \frac{\sigma_D}{D}. \quad (22)$$

Equations (16), (17), (21), and (22) will finally be utilized for obtaining the contour plots between  $\Omega_{k0}$  and  $H_0$  at different confidence levels.

Finally we constrain the curvature density parameter  $\Omega_{k0}$  and the Hubble parameter  $H_0$  simultaneously by minimizing the  $\chi^2$  statistics. The  $\chi^2$  function is given by,

$$\chi^2 = \Delta\mu^T \mathbf{\Sigma}^{-1} \Delta\mu. \quad (23)$$

$\Delta\mu = \mu_{\text{SN}} - \mu_H$  is the difference between the distance moduli of Pantheon SN-Ia and that of the  $H(z)$  data.  $\mathbf{\Sigma} = \sigma_{\mu_{\text{SN}}}^2 + \sigma_{\mu_H}^2$  is the total uncertainty matrix from combined Pantheon and Hubble data.

We attempt to reconstruct  $\Omega_{k0}$  directly for the following combination of datasets,

(1) Set I

- (a) N1—CC + SN
- (b) P1—CC + SN + P18
- (c) R1—CC + SN + R19

(2) Set II

- (a) N2—CC +  $r$ BAO + SN
- (b) P2—CC +  $r$ BAO + SN + P18
- (c) R2—CC +  $r$ BAO + SN + R19

We get the constraints on  $\Omega_{k0}$  and  $H_0$  along with their respective error uncertainties by a Markov Chain Monte Carlo (MCMC) analysis with the assumption of a uniform prior distribution for  $\Omega_{k0} \in [-1, 1]$  and  $H_0 \in [50, 100]$  in case of the N1 and N2 combinations respectively. For the P1 and P2 combinations, we consider the P18 Gaussian  $H_0$  prior whereas, for R1 and R2 combinations, the R19 Gaussian  $H_0$  prior has been used.

In this work, we adopt a python implementation of the ensemble sampler for MCMC, the publicly available EMCEE,<sup>3</sup> introduced by Foreman-Mackey *et al.* [112]. The best fit results along with their respective  $1\sigma$ ,  $2\sigma$ , and  $3\sigma$  uncertainties is given in Table I. We plot the results using the GETDIST<sup>4</sup> module of python, developed by Lewis [113]. The plots for the marginalized distributions with  $1\sigma$  and  $2\sigma$  confidence contours for  $\Omega_{k0}$  and  $H_0$  are shown in Figs. 1, 2, 3, and 4 considering the squared exponential, Matérn 9/2, Cauchy and rational quadratic covariance respectively.

The reconstructed  $\Omega_{k0}$  for the N1 combination are consistent with spatial flatness within  $2\sigma$  confidence level (CL) for the squared exponential, Matérn 9/2 and Cauchy covariance functions, and within  $3\sigma$  CL for the rational quadratic covariance. With the addition of  $r$ BAO data in Set II, the constraints on  $\Omega_{k0}$  become tighter. From the combined N2 dataset, we find that  $\Omega_{k0}$  is consistent with a spatially flat universe at  $1\sigma$  CL for the squared exponential, Matérn 9/2 and Cauchy covariance, whereas in  $2\sigma$  for the rational quadratic kernel. The best-fit values shows an inclination toward a closed universe for N1 and N2 datasets. The degeneracy between  $H_0$  and  $\Omega_{k0}$  along with their correlation has also been shown.

We also examine if the two different strategies for determining value of  $H_0$ , with conflicting results, affect the reconstruction significantly. We plot the marginalized distributions with  $1\sigma$  and  $2\sigma$  confidence contours for  $\Omega_{k0}$  and  $H_0$  using the P1 and P2 combinations considering the P18 prior on  $H_0$ , and for the R1 and R2 combinations considering the R19 prior on  $H_0$  in Figs. 1–4. With the inclusion of the P18 data prior we see that the best-fit values of  $\Omega_{k0}$  favor a spatially open universe, whereas in case of the choice of R19 as a prior, the best-fit values of the constrained  $\Omega_{k0}$  shows that the combined data favors a spatially closed universe. However, a spatially flat universe is mostly included at  $2\sigma$  CL for both cases.

<sup>3</sup><https://github.com/dfm/emcee>.

<sup>4</sup><https://github.com/cmbant/getdist>.

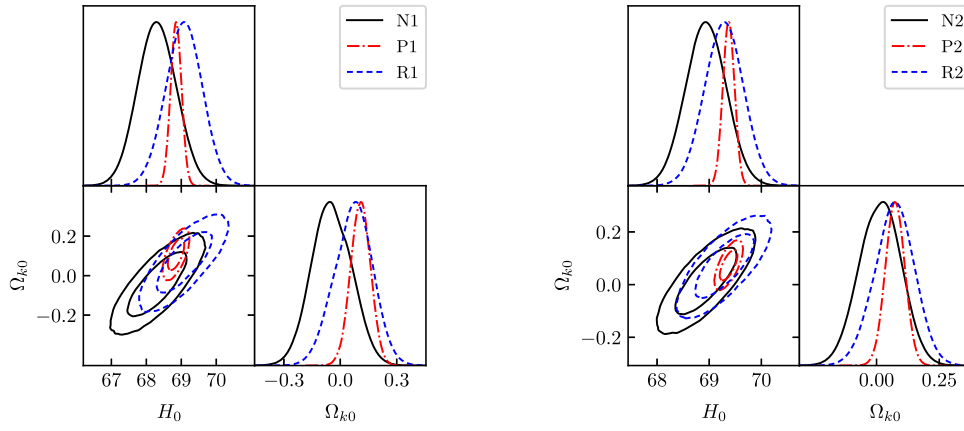


FIG. 1. Contour plots and the marginalized likelihood of  $H_0$  and  $\Omega_{k_0}$  considering the squared exponential covariance for Set I (left) and Set II (right). The solid lines represent the results for N1 and N2 dataset combination, dash-dot lines corresponds to the P1 and P2 dataset combination, and the dashed lines represent the results for R1 and R2 dataset combinations. The associated  $1\sigma$ ,  $2\sigma$  confidence contours are shown along with the respective marginalized likelihood functions.

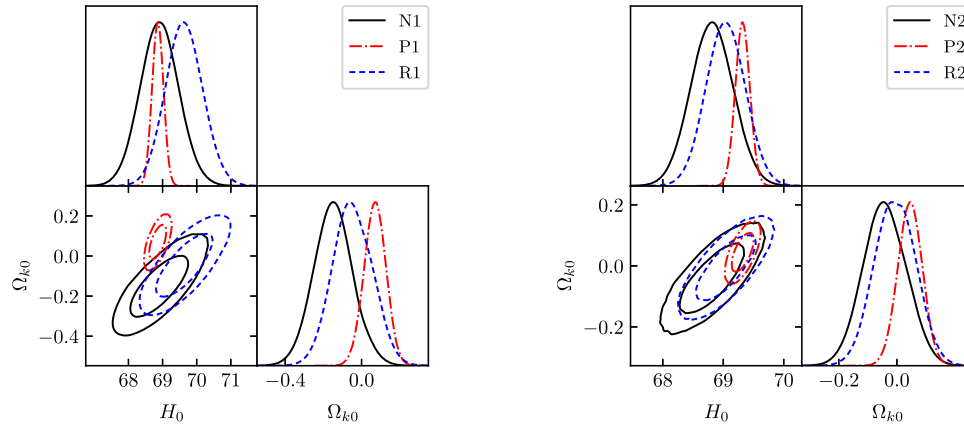


FIG. 2. Contour plots and the marginalized likelihood of  $H_0$  and  $\Omega_{k_0}$  considering the Matérn 9/2 covariance for Set I (left) and Set II (right). The solid lines represent the results for N1 and N2 dataset combination, dash-dot lines corresponds to the P1 and P2 dataset combination, and the dashed lines represent the results for R1 and R2 dataset combinations. The associated  $1\sigma$ ,  $2\sigma$  confidence contours are shown along with the respective marginalized likelihood functions.

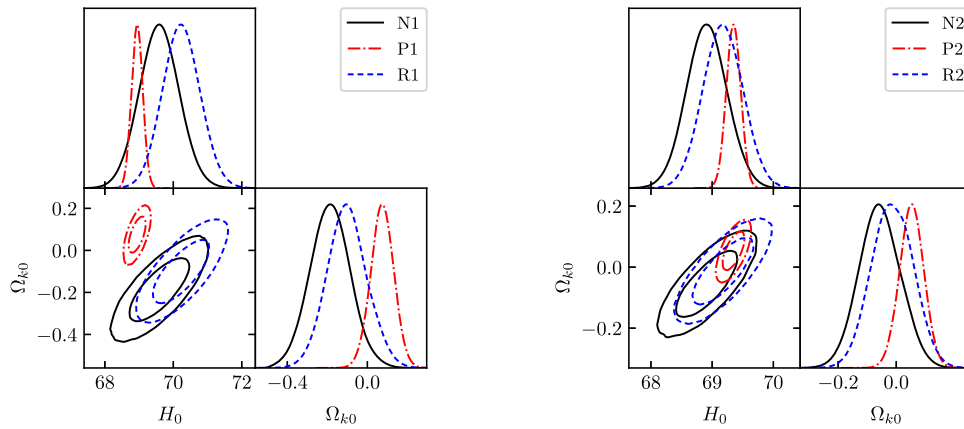


FIG. 3. Contour plots and the marginalized likelihood of  $H_0$  and  $\Omega_{k_0}$  considering the Cauchy covariance for Set I (left) and Set II (right). The solid lines represent the results for N1 and N2 dataset combination, dash-dot lines corresponds to the P1 and P2 dataset combination, and the dashed lines represent the results for R1 and R2 dataset combinations. The associated  $1\sigma$ ,  $2\sigma$  confidence contours are shown along with the respective marginalized likelihood functions.

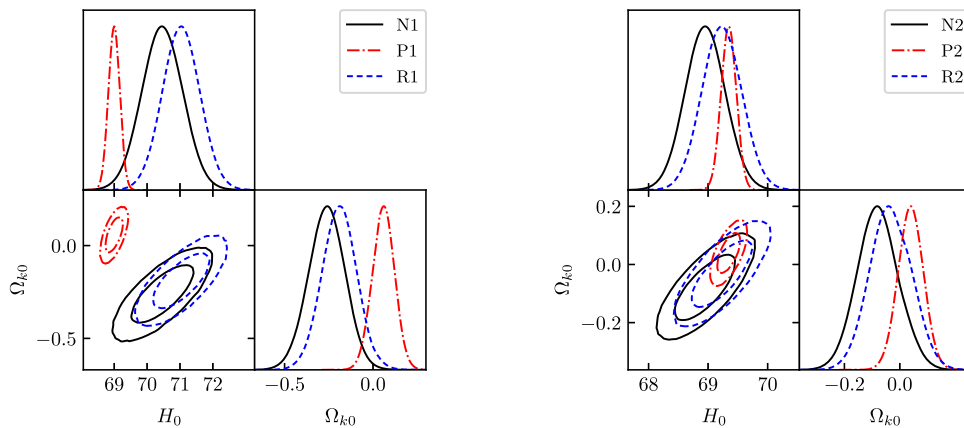


FIG. 4. Contour plots and the marginalized likelihood of  $H_0$  and  $\Omega_{k0}$  considering the rational quadratic covariance for Set I (left) and Set II (right). The solid lines represent the results for N1 and N2 dataset combination, dash-dot lines corresponds to the P1 and P2 dataset combination, and the dashed lines represent the results for R1 and R2 dataset combinations. The associated  $1\sigma$ ,  $2\sigma$  confidence contours are shown along with the respective marginalized likelihood functions.

## VI. THERMODYNAMIC CONSISTENCY OF $\Omega_{k0}$ CONSTRAINTS

In this section, the consistency of constraints obtained on  $\Omega_{k0}$  with the second law of thermodynamics is looked at. We assume the universe as a system is bounded by a cosmological horizon, and the matter content of the universe is enclosed within a volume defined by a radius not bigger than the horizon [114–116]. In cosmology, the apparent horizon  $r_A$  serves as the cosmological horizon, which is given by the equation  $g^{\mu\nu}R_{,\mu}R_{,\nu} = 0$ , where  $R = a(t)r$  is the proper radius of the 2-sphere and  $r$  is the comoving radius. For the FLRW universe with a spatial curvature index  $k$ , the apparent horizon is thus given by

$$r_A = \left( H^2 + \frac{k}{a^2} \right)^{-\frac{1}{2}}. \quad (24)$$

For  $k = 0$ , the apparent horizon reduces to the Hubble horizon  $r_H = \frac{1}{H}$ .

Now, the entropy of the horizon  $S_A$  can be written as [117],

$$S_A = 8\pi^2 r_A^2 = \frac{8\pi^2}{H^2 + \frac{k}{a^2}}. \quad (25)$$

For the second law to be valid, the entropy  $S$  should be nondecreasing with respect to the expansion of the universe. If  $S_f$  and  $S_A$  stand for the entropy of the fluid describing the observable universe, and that of the horizon containing the fluid, respectively, then the total entropy of the system, i.e.,  $S = S_f + S_A$ , should satisfy the relation

$$\frac{dS}{da} \equiv \frac{dS_f}{da} + \frac{dS_A}{da} \geq 0. \quad (26)$$

Recently Ferreira and Pavón [35] gave a prescription to ascertain the signature of  $k$  from the second law of thermodynamics. It is a fair assumption that the entropy of the observable universe is dominated by that of the cosmic horizon  $S_A$  [118]. So, the second law can be safely written as [35],

$$\frac{dS_A}{da} \geq 0. \quad (27)$$

Using Eq. (25) in (27) one can obtain the following condition,

$$H \frac{dH}{da} \leq \frac{k}{a^3}. \quad (28)$$

The inequality (28) can be rewritten, with a bit of simple algebraic exercise, as

$$1 + q \geq \Omega_k. \quad (29)$$

Here  $q$  is the deceleration parameter which gives a dimensionless measure of the cosmic acceleration and is defined as,

$$q = -\frac{\ddot{a}}{aH^2} = -1 + (1+z)\frac{H'}{H}. \quad (30)$$

Testing the thermodynamic validity for the obtained constraints on  $\Omega_{k0}$  requires a reconstruction of  $q_0$  from the respective combination of datasets. Quite a lot of work on a nonparametric reconstruction of the cosmic deceleration parameter  $q$  is already there in the literature. Some of them

can be found in [50–54,56]. The list, however, is far from being exhaustive. We use the same datasets, that were used for the reconstruction of  $\Omega_{k0}$ , to find the corresponding values of  $q_0$ . A very brief methodology is the following. For a more detailed technical description, we refer to [50,57]. The comoving distance  $D(z)$ , and its derivatives  $D'(z)$  and  $D''(z)$  are reconstructed with respect to  $z$  for different combinations of datasets. The uncertainty in  $D(z)$  from the corresponding dataset is taken into account. For the CC and  $r$ BAO data, we convert the  $H - \sigma_H$  data to  $E - \sigma_E$  dataset using Eqs. (9) and (13).  $D'(z)$  is then connected to  $D(z)$  and  $E(z)$  via Eq. (12) as,

$$D'(z) = \frac{\sqrt{1 + \Omega_{k0} D^2(z)}}{E(z)}. \quad (31)$$

Thus, we take into account the  $E$  data points, the uncertainty associated  $\sigma_E$  while performing the GP

reconstruction. We add two extra points  $D(0) = 0$  to the  $D$  dataset, and  $E(0) = 1$  to the  $E$  data before proceeding with the reconstruction. We obtain the reconstructed values of  $D(z)$ ,  $D'(z)$  and  $D''(z)$  at the present epoch, along with their error uncertainties. Now,  $q$  can be rewritten as a function of  $D(z)$  and its derivatives as,

$$q(z) = -1 + \frac{\Omega_{k0} D D^2 - (1 + \Omega_{k0} D^2) D''}{D'(1 + \Omega_{k0} D^2)} (1 + z). \quad (32)$$

Using the reconstructed  $D(0)$ ,  $D'(0)$ , and  $D''(0)$ , we obtain the values of  $1 + q_0$ , shown in the third column of Table I. Equation (29) asserts that  $\Omega_{k0} \leq 1 + q_0$  for the second law to be valid. We see that for all combinations, the second law is satisfied by a generous margin, independent of the choice of the kernel.

TABLE I. The best fit values of  $\Omega_{k0}$ ,  $H_0$ , and reconstructed  $1 + q_0$  along with their  $1\sigma$ ,  $2\sigma$ , and  $3\sigma$  uncertainties from different combinations of datasets, for four choices of the covariance function using the background data.

Dataset	$\kappa(z, \tilde{z})$	$H_0$	$\Omega_{k0}$	$1 + q_0$	
N1	Squared Exponential	$68.30^{+0.56+1.09+1.67}_{-0.55-1.06-1.59}$	$-0.05^{+0.11+0.21+0.32}_{-0.10-0.20-0.31}$	$0.49^{+0.06+0.12+0.18}_{-0.06-0.13-0.19}$	
N2		$68.94^{+0.39+0.76+1.15}_{-0.39-0.75-1.14}$	$0.02^{+0.08+0.16+0.24}_{-0.09-0.16-0.25}$	$0.42^{+0.03+0.06+0.09}_{-0.03-0.06-0.09}$	
P1		$68.85^{+0.16+0.31+0.46}_{-0.16-0.31-0.46}$	$0.11^{+0.05+0.11+0.16}_{-0.05-0.11-0.16}$	$0.46^{+0.06+0.12+0.18}_{-0.06-0.12-0.18}$	
P2		$69.37^{+0.11+0.22+0.33}_{-0.11-0.22-0.33}$	$0.07^{+0.04+0.08+0.12}_{-0.04-0.08-0.12}$	$0.39^{+0.03+0.06+0.10}_{-0.03-0.06-0.10}$	
R1		$69.08^{+0.52+1.02+1.54}_{-0.52-1.03-1.55}$	$0.07^{+0.10+0.19+0.29}_{-0.11-0.21-0.31}$	$0.45^{+0.06+0.12+0.18}_{-0.06-0.12-0.18}$	
R2		$69.29^{+0.37+0.72+1.10}_{-0.37-0.73-1.10}$	$0.07^{+0.08+0.15+0.23}_{-0.08-0.16-0.24}$	$0.40^{+0.03+0.06+0.09}_{-0.03-0.06-0.09}$	
N1		Matérn 9/2	$68.91^{+0.56+1.13+1.72}_{-0.56-1.10-1.65}$	$-0.15^{+0.10+0.21+0.32}_{-0.10-0.20-0.31}$	$0.50^{+0.05+0.11+0.15}_{-0.05-0.10-0.16}$
N2			$68.81^{+0.35+0.69+1.06}_{-0.35-0.68-1.03}$	$-0.04^{+0.08+0.15+0.22}_{-0.07-0.14-0.22}$	$0.43^{+0.05+0.09+0.14}_{-0.05-0.09-0.14}$
P1	$68.86^{+0.17+0.33+0.49}_{-0.17-0.33-0.49}$		$0.07^{+0.06+0.11+0.17}_{-0.06-0.11-0.17}$	$0.51^{+0.05+0.10+0.15}_{-0.05-0.10-0.15}$	
P2	$69.32^{+0.12+0.24+0.36}_{-0.12-0.24-0.36}$		$0.05^{+0.04+0.08+0.12}_{-0.04-0.08-0.13}$	$0.40^{+0.04+0.08+0.13}_{-0.04-0.08-0.13}$	
R1	$68.63^{+0.55+1.09+1.64}_{-0.53-1.04-1.57}$		$-0.05^{+0.11+0.21+0.31}_{-0.10-0.20-0.30}$	$0.52^{+0.05+0.12+0.17}_{-0.05-0.11-0.16}$	
R2	$69.04^{+0.32+0.64+0.96}_{-0.32-0.63-0.95}$		$-0.01^{+0.07+0.14+0.21}_{-0.07-0.14-0.21}$	$0.43^{+0.04+0.08+0.12}_{-0.04-0.08-0.12}$	
N1	Cauchy		$69.59^{+0.58+1.15+1.77}_{-0.57-1.13-1.68}$	$-0.19^{+0.10+0.20+0.31}_{-0.10-0.20-0.29}$	$0.41^{+0.07+0.13+0.20}_{-0.07-0.13-0.21}$
N2			$68.91^{+0.33+0.66+0.99}_{-0.33-0.64-0.97}$	$-0.06^{+0.07+0.14+0.21}_{-0.07-0.14-0.21}$	$0.41^{+0.04+0.07+0.11}_{-0.04-0.07-0.11}$
P1		$68.94^{+0.16+0.32+0.49}_{-0.16-0.32-0.49}$	$0.07^{+0.06+0.11+0.17}_{-0.06-0.12-0.17}$	$0.45^{+0.07+0.13+0.19}_{-0.07-0.14-0.19}$	
P2		$69.35^{+0.12+0.23+0.35}_{-0.12-0.23-0.35}$	$0.05^{+0.04+0.08+0.12}_{-0.04-0.08-0.13}$	$0.38^{+0.04+0.07+0.11}_{-0.04-0.07-0.11}$	
R1		$70.23^{+0.55+1.09+1.67}_{-0.54-1.06-1.59}$	$-0.10^{+0.10+0.20+0.30}_{-0.10-0.19-0.29}$	$0.38^{+0.07+0.15+0.21}_{-0.07-0.14-0.20}$	
R2		$69.18^{+0.33+0.64+0.96}_{-0.32-0.63-0.95}$	$-0.01^{+0.07+0.14+0.21}_{-0.07-0.14-0.21}$	$0.39^{+0.04+0.07+0.11}_{-0.04-0.07-0.11}$	
N1		Rational Quadratic	$70.46^{+0.62+1.22+1.87}_{-0.62-1.21-1.83}$	$-0.26^{+0.10+0.20+0.31}_{-0.10-0.21-0.31}$	$0.37^{+0.07+0.14+0.20}_{-0.07-0.13-0.20}$
N2			$68.95^{+0.34+0.67+1.02}_{-0.33-0.65-0.99}$	$-0.08^{+0.08+0.15+0.22}_{-0.07-0.14-0.22}$	$0.41^{+0.04+0.07+0.11}_{-0.04-0.08-0.11}$
P1	$68.99^{+0.17+0.34+0.52}_{-0.17-0.34-0.52}$		$0.06^{+0.06+0.12+0.18}_{-0.06-0.12-0.19}$	$0.45^{+0.07+0.13+0.20}_{-0.07-0.13-0.20}$	
P2	$69.35^{+0.13+0.25+0.38}_{-0.13-0.25-0.38}$		$0.04^{+0.05+0.09+0.14}_{-0.05-0.09-0.14}$	$0.38^{+0.04+0.08+0.12}_{-0.04-0.08-0.12}$	
R1	$71.03^{+0.57+1.22+1.70}_{-0.56-1.11-1.68}$		$-0.19^{+0.10+0.20+0.30}_{-0.10-0.20-0.30}$	$0.37^{+0.06+0.12+0.17}_{-0.06-0.12-0.17}$	
R2	$69.23^{+0.34+0.66+1.00}_{-0.33-0.64-0.97}$		$-0.03^{+0.08+0.15+0.22}_{-0.07-0.14-0.22}$	$0.39^{+0.04+0.07+0.11}_{-0.04-0.07-0.11}$	



## VII. RECONSTRUCTION ALONG WITH THE PERTURBATION DATA

Redshift-space distortions are an effect in observational cosmology where the spatial distribution of galaxies appears distorted when their positions are looked at as a function of their redshift, rather than as functions of their distances. This effect occurs due to the peculiar velocities of the galaxies causing a Doppler shift in addition to the redshift caused by the cosmological expansion. The growth of large structure can not only probe the background evolution of the universe, but also distinguish between GR and different modified gravity theories [119,120]. Recently, nonparametric constraints on the Hubble parameter  $H$  and the matter density parameter  $\Omega_m$  were obtained using the data from cosmic chronometers, type-Ia supernovae, baryon acoustic oscillations and redshift-space distortions, assuming a spatially flat universe [121]. In this section, we propose a nonparametric method to use the growth rate data measured from RSDs to constrain the spatial curvature.

In a background universe filled with matter and dark energy, the evolution of matter density contrast is given by,

$$\delta = \frac{\delta\rho_m}{\rho_m}. \quad (33)$$

In the linearized approximation,  $\delta$  obeys the following second order differential equation for its evolution,

$$\ddot{\delta} + 2H\dot{\delta} - 4\pi G_{\text{eff}}\rho_m\delta = 0, \quad (34)$$

where  $\rho_m$  is the background matter density,  $\delta\rho_m$  represents its first-order perturbation, and the ‘‘dot’’ denotes derivative with respect to cosmic time  $t$ . Note that  $G_{\text{eff}}$  is the effective gravitational constant. For Einstein’s GR,  $G_{\text{eff}}$  reduces to the Newton’s gravitational constant  $G$ . Considering the growth factor  $f(a) = \frac{d \ln \delta}{d \ln a}$ , Gong *et al.* [122] provided an approximate solution to Eq. (34) as,

$$f(z) = \Omega_m^\gamma + \left(\gamma - \frac{4}{7}\right)\Omega_k. \quad (35)$$

Here,  $\Omega_m = \frac{\Omega_{m0}(1+z)^3}{E^2(z)}$  is the matter density parameter,  $\Omega_k = \frac{\Omega_{k0}(1+z)^2}{E^2(z)}$  is the curvature density parameter and  $E(z) = \frac{H(z)}{H_0}$ . The growth index  $\gamma$  depends on the model. For the  $\Lambda$ CDM model,  $f(z) \simeq \Omega_m^\gamma$ , and  $\gamma = 6/11$  is a solution to Eq. (34) where the terms  $\mathcal{O}(1 - \Omega_m)^2$  are neglected [123]. For dark energy models with slowly varying equation of state  $\gamma \simeq 0.55$  [124]. For modified gravity models, different values have been predicted in literature, such as  $\gamma \simeq 0.68$  for Dvali-Gabadadze-Porrati (DGP) model [125,126]. The RSD data measure the quantity  $f\sigma_8$ , defined by,

$$\begin{aligned} f\sigma_8(z) &= f(z)\sigma_{8,0} \frac{\delta(z)}{\delta_0}, \\ &= \sigma_{8,0} f(z) \exp \left\{ \int_0^z -\frac{f(z')}{1+z'} dz' \right\}, \end{aligned} \quad (36)$$

where  $\sigma_8$  is the linear theory root-mean-square mass fluctuation within a sphere of radius  $8h^{-1}$  Mpc [127–131],  $h$  being the dimensionless Hubble parameter at the present epoch.

On substituting Eq. (35) in (36) we get,

$$\begin{aligned} f\sigma_8(z) &= \sigma_{8,0} \left[ \Omega_m^\gamma + \left(\gamma - \frac{4}{7}\right)\Omega_k \right] \\ &\times \exp \left\{ \int_0^z -\frac{[\Omega_m^\gamma + (\gamma - \frac{4}{7})\Omega_k]}{1+z'} dz' \right\}. \end{aligned} \quad (37)$$

We proceed with the integration of Eq. (37) numerically using the composite trapezoidal rule as in Eq. (14). The reconstructed  $E(z)$  function from CC and CC +  $r$ BAO data are considered. For the Pantheon data, we make use of Eqs. (16) and (17).

Here we consider the following combination of datasets,

- (1) Set III
  - (a) N3—CC + SN + RSD
  - (b) P3—CC + SN + RSD + P18
  - (c) R3—CC + SN + RSD + R19
- (2) Set IV
  - (a) N4—CC +  $r$ BAO + SN + RSD
  - (b) P4—CC +  $r$ BAO + SN + RSD + P18
  - (c) R4—CC +  $r$ BAO + SN + RSD + R19

We use the GP method to reconstruct the function  $f\sigma_8(z)$  from RSD data. Finally, we constrain the cosmological parameters  $\Omega_{m0}$ ,  $\Omega_{k0}$ ,  $\sigma_{8,0}$ , and  $\gamma$  utilizing the  $\chi^2$  minimization technique. The uncertainties associated are estimated via a Markov Chain Monte Carlo analysis. The best fit results along with their respective  $1\sigma$ ,  $2\sigma$ , and  $3\sigma$  uncertainties is given in Table II. Plots for the marginalized posteriors with  $1\sigma$  and  $2\sigma$  confidence contours using the Set III and Set IV data combinations are shown in Figs. 5, 6, 7, and 8, for the squared exponential, Matérn 9/2, Cauchy and rational quadratic covariance respectively.

The marginalized  $\Omega_{k0}$  constraints for the N3 combination is consistent with spatial flatness within  $1\sigma$  CL for the squared exponential and Matérn 9/2 covariance, within  $2\sigma$  for the Cauchy covariance and within  $3\sigma$  for the rational quadratic covariance. For the N4 combination, reconstructed  $\Omega_{k0}$  lies with  $1\sigma$  for all four kernel choices. Considering the P18 and R19  $H_0$  prior, it is seen that the squared exponential kernel includes  $\Omega_{k0} = 0$  for P3, P4, R4 combinations within  $1\sigma$  and for the R3 combination within  $2\sigma$ . The Matérn 9/2 kernel includes  $\Omega_{k0} = 0$  for all P3, P4, R3, R4 combinations within  $1\sigma$ . The Cauchy kernel includes  $\Omega_{k0} = 0$  for the P3, R3 combination in  $2\sigma$ , and for the P4, R4 combination in  $1\sigma$  CL. Lastly, utilizing the

TABLE II. The best fit values of  $\Omega_{m0}$ ,  $\Omega_{k0}$ ,  $\sigma_{8,0}$ , and  $\gamma$  along with their  $1\sigma$ ,  $2\sigma$ , and  $3\sigma$  uncertainties from different combinations of datasets for four choices of the covariance function using the background and perturbation data.

Set	$\kappa(z, \tilde{z})$	$\Omega_{m0}$	$\Omega_{k0}$	$\sigma_{8,0}$	$\gamma$
N3		$0.204^{+0.042+0.082+0.126}_{-0.041-0.079-0.121}$	$0.040^{+0.152+0.285+0.419}_{-0.161-0.313-0.483}$	$0.952^{+0.074+0.163+0.296}_{-0.063-0.116-0.171}$	$0.629^{+0.053+0.139+0.311}_{-0.045-0.094-0.148}$
N4		$0.196^{+0.023+0.044+0.068}_{-0.023-0.045-0.065}$	$-0.097^{+0.105+0.205+0.299}_{-0.102-0.202-0.314}$	$0.964^{+0.039+0.082+0.120}_{-0.034-0.063-0.090}$	$0.619^{+0.020+0.040+0.066}_{-0.020-0.041-0.079}$
P3	Squared	$0.199^{+0.042+0.083+0.125}_{-0.041-0.075-0.099}$	$0.077^{+0.084+0.159+0.212}_{-0.091-0.178-0.265}$	$0.961^{+0.077+0.159+0.232}_{-0.065-0.118-0.164}$	$0.626^{+0.049+0.102+0.174}_{-0.049-0.095-0.132}$
P4	Exponential	$0.185^{+0.021+0.041+0.066}_{-0.021-0.043-0.063}$	$0.007^{+0.065+0.127+0.218}_{-0.063-0.122-0.186}$	$0.976^{+0.040+0.089+0.141}_{-0.036-0.067-0.100}$	$0.618^{+0.023+0.047+0.103}_{-0.023-0.050-0.078}$
R3		$0.203^{+0.032+0.064+0.096}_{-0.033-0.064-0.108}$	$0.078^{+0.073+0.144+0.212}_{-0.077-0.155-0.232}$	$0.885^{+0.063+0.132+0.250}_{-0.052-0.098-0.144}$	$0.688^{+0.058+0.139+0.278}_{-0.050-0.098-0.156}$
R4		$0.159^{+0.020+0.042+0.077}_{-0.021-0.041-0.056}$	$0.005^{+0.061+0.115+0.171}_{-0.060-0.119-0.228}$	$0.963^{+0.045+0.097+0.148}_{-0.040-0.076-0.117}$	$0.625^{+0.026+0.052+0.079}_{-0.027-0.056-0.081}$
N3		$0.227^{+0.041+0.079+0.117}_{-0.040-0.074-0.105}$	$-0.110^{+0.155+0.307+0.445}_{-0.155-0.312-0.498}$	$0.897^{+0.057+0.118+0.183}_{-0.048-0.089-0.125}$	$0.615^{+0.036+0.072+0.118}_{-0.034-0.066-0.097}$
N4		$0.227^{+0.027+0.053+0.079}_{-0.026-0.049-0.074}$	$-0.026^{+0.104+0.202+0.297}_{-0.104-0.215-0.322}$	$0.897^{+0.039+0.076+0.125}_{-0.034-0.064-0.090}$	$0.633^{+0.025+0.052+0.082}_{-0.026-0.050-0.078}$
P3	Matérn	$0.228^{+0.038+0.077+0.114}_{-0.038-0.077-0.108}$	$-0.044^{+0.089+0.175+0.264}_{-0.090-0.176-0.270}$	$0.903^{+0.055+0.125+0.195}_{-0.048-0.091-0.127}$	$0.615^{+0.037+0.073+0.114}_{-0.035-0.073-0.107}$
P4	9/2	$0.221^{+0.025+0.049+0.076}_{-0.024-0.047-0.066}$	$0.018^{+0.067+0.128+0.185}_{-0.067-0.131-0.196}$	$0.902^{+0.038+0.077+0.115}_{-0.035-0.065-0.095}$	$0.632^{+0.027+0.054+0.083}_{-0.026-0.051-0.072}$
R3		$0.220^{+0.032+0.064+0.100}_{-0.032-0.062-0.093}$	$-0.031^{+0.083+0.159+0.235}_{-0.081-0.159-0.242}$	$0.853^{+0.048+0.102+0.171}_{-0.042-0.079-0.115}$	$0.651^{+0.039+0.080+0.125}_{-0.036-0.070-0.107}$
R4		$0.178^{+0.024+0.049+0.076}_{-0.023-0.045-0.065}$	$0.034^{+0.065+0.124+0.177}_{-0.063-0.123-0.188}$	$0.907^{+0.046+0.096+0.147}_{-0.040-0.076-0.110}$	$0.629^{+0.031+0.061+0.093}_{-0.030-0.061-0.094}$
N3		$0.245^{+0.040+0.078+0.120}_{-0.038-0.073-0.115}$	$-0.227^{+0.146+0.291+0.426}_{-0.164-0.318-0.494}$	$0.855^{+0.047+0.099+0.169}_{-0.041-0.075-0.107}$	$0.608^{+0.029+0.059+0.089}_{-0.029-0.056-0.091}$
N4		$0.278^{+0.027+0.053+0.080}_{-0.026-0.050-0.076}$	$-0.015^{+0.104+0.198+0.295}_{-0.108-0.208-0.314}$	$0.820^{+0.029+0.061+0.097}_{-0.028-0.052-0.076}$	$0.663^{+0.028+0.060+0.099}_{-0.026-0.048-0.071}$
P3		$0.246^{+0.039+0.076+0.115}_{-0.039-0.082-0.132}$	$-0.137^{+0.092+0.183+0.285}_{-0.091-0.180-0.273}$	$0.868^{+0.049+0.114+0.229}_{-0.042-0.077-0.110}$	$0.602^{+0.031+0.062+0.098}_{-0.031-0.065-0.127}$
P4	Cauchy	$0.275^{+0.024+0.048+0.073}_{-0.024-0.047-0.071}$	$0.017^{+0.063+0.124+0.183}_{-0.067-0.130-0.196}$	$0.821^{+0.029+0.060+0.095}_{-0.027-0.051-0.075}$	$0.665^{+0.027+0.055+0.086}_{-0.026-0.050-0.074}$
R3		$0.238^{+0.032+0.063+0.092}_{-0.032-0.063-0.092}$	$-0.123^{+0.081+0.159+0.246}_{-0.080-0.161-0.243}$	$0.823^{+0.041+0.087+0.136}_{-0.036-0.067-0.096}$	$0.633^{+0.031+0.061+0.097}_{-0.030-0.059-0.090}$
R4		$0.236^{+0.024+0.048+0.072}_{-0.024-0.045-0.072}$	$0.022^{+0.059+0.115+0.169}_{-0.061-0.119-0.179}$	$0.807^{+0.033+0.067+0.112}_{-0.030-0.057-0.083}$	$0.679^{+0.031+0.063+0.102}_{-0.030-0.058-0.092}$
N3		$0.271^{+0.039+0.079+0.120}_{-0.040-0.079-0.118}$	$-0.305^{+0.155+0.298+0.453}_{-0.163-0.333-0.509}$	$0.799^{+0.039+0.083+0.133}_{-0.034-0.064-0.094}$	$0.599^{+0.025+0.051+0.096}_{-0.024-0.049-0.075}$
N4		$0.426^{+0.045+0.090+0.135}_{-0.045-0.090-0.169}$	$0.049^{+0.117+0.236+0.375}_{-0.121-0.235-0.351}$	$0.657^{+0.027+0.057+0.095}_{-0.024-0.045-0.066}$	$0.819^{+0.050+0.118+0.239}_{-0.042-0.081-0.119}$
P3	Rational	$0.280^{+0.040+0.078+0.119}_{-0.040-0.078-0.124}$	$-0.186^{+0.096+0.184+0.269}_{-0.098-0.191-0.292}$	$0.811^{+0.039+0.082+0.141}_{-0.035-0.063-0.092}$	$0.594^{+0.026+0.053+0.082}_{-0.026-0.052-0.082}$
P4	Quadratic	$0.367^{+0.024+0.048+0.073}_{-0.024-0.047-0.072}$	$0.110^{+0.070+0.140+0.208}_{-0.070-0.140-0.218}$	$0.703^{+0.024+0.048+0.074}_{-0.022-0.043-0.063}$	$0.766^{+0.045+0.101+0.167}_{-0.038-0.071-0.103}$
R3		$0.265^{+0.032+0.062+0.097}_{-0.032-0.063-0.092}$	$-0.162^{+0.085+0.165+0.250}_{-0.090-0.179-0.267}$	$0.777^{+0.033+0.069+0.107}_{-0.030-0.055-0.083}$	$0.618^{+0.025+0.050+0.080}_{-0.025-0.049-0.073}$
R4		$0.331^{+0.024+0.047+0.070}_{-0.024-0.047-0.069}$	$0.082^{+0.062+0.124+0.182}_{-0.062-0.124-0.185}$	$0.672^{+0.023+0.047+0.075}_{-0.022-0.042-0.060}$	$0.807^{+0.050+0.109+0.170}_{-0.041-0.076-0.110}$

rational quadratic kernel,  $\Omega_{k0} = 0$  is included in  $3\sigma$  for the P3 and R3 combination, whereas in  $2\sigma$  for the P4, R4 combination. Inclusion of  $r$ BAO data leads to tighter constraints on  $\Omega_{k0}$ , and the best-fit values are seen to favor a spatially open universe (see Table II).

The reconstructed values of  $\gamma$  show that the  $\Lambda$ CDM model is mostly included in  $2\sigma$  and always in  $3\sigma$ , except for the rational quadratic kernel. From Table II, it can be seen that for the N4, P4, and R4 combinations, the  $\Lambda$ CDM model is not included in  $3\sigma$  considering the rational quadratic kernel, and marginally included in  $3\sigma$  while using the Cauchy covariance.

## VIII. DISCUSSION

In the present work, constraints on the cosmic curvature density parameter  $\Omega_{k0}$  have been obtained from different cosmological probes with the help of a nonparametric reconstruction. The cosmic chronometer and the radial

baryon acoustic oscillation measurements of the Hubble parameter, the recent supernova compilation of the corrected Pantheon sample, along with measurement of the redshift space distortions which measure the growth of large structure are utilized for the purpose. The widely used Gaussian process and the Markov Chain Monte Carlo method have been employed in this work. The analysis has been performed for four choices of the covariance function, namely the squared exponential, Matérn 9/2, Cauchy and rational quadratic kernel. The choice of covariance function involves some discretion and thus a bit subjective. The use of various choices of covariance makes the present investigation quite exhaustive in that respect.

The reconstructed  $\Omega_{k0}$  obtained by combining the CC and Pantheon data are consistent with spatial flatness within  $1\sigma$  confidence level for the squared exponential covariance function, within  $2\sigma$  CL level for the Matérn 9/2 and Cauchy covariance function, and within  $3\sigma$  CL for the rational quadratic covariance. Including the  $r$ BAO data to

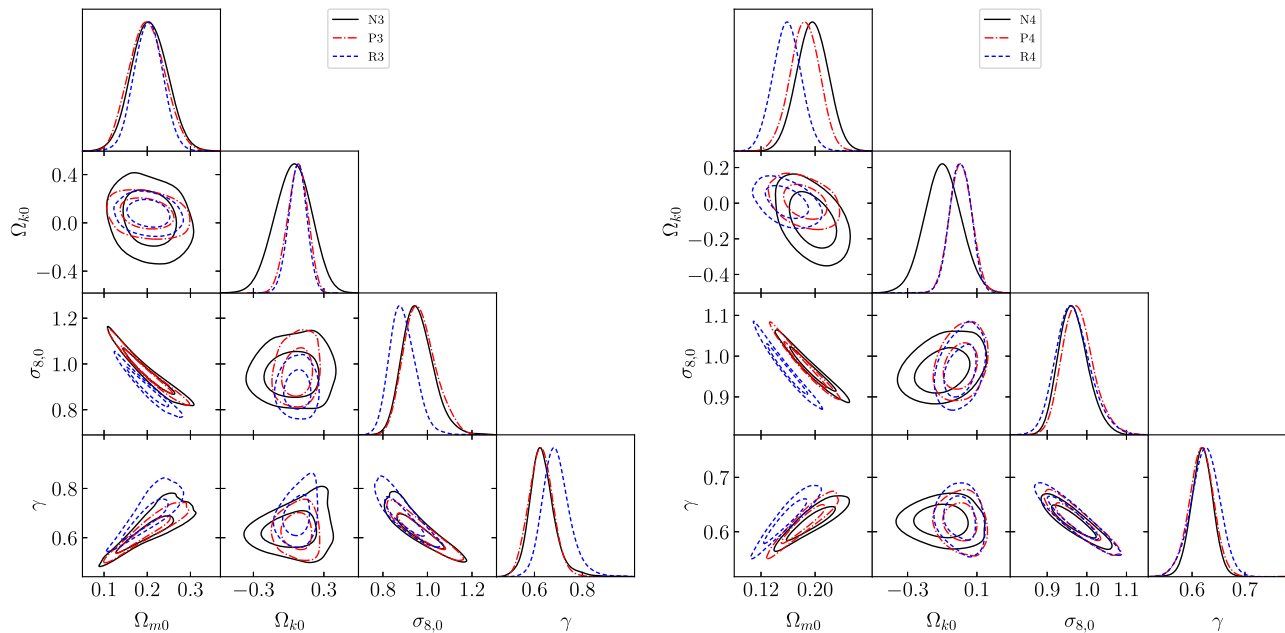


FIG. 5. Contour plots and the marginalized likelihood of  $H_0$  and  $\Omega_{k0}$  considering the squared exponential covariance for Set III (left) and Set IV (right). The solid lines represent the results for N3 and N4 dataset combination, dash-dot lines corresponds to the P3 and P4 dataset combination, and the dashed lines represent the results for R3 and R4 dataset combinations. The associated  $1\sigma$ ,  $2\sigma$  confidence contours are shown along with the respective marginalized likelihood functions.

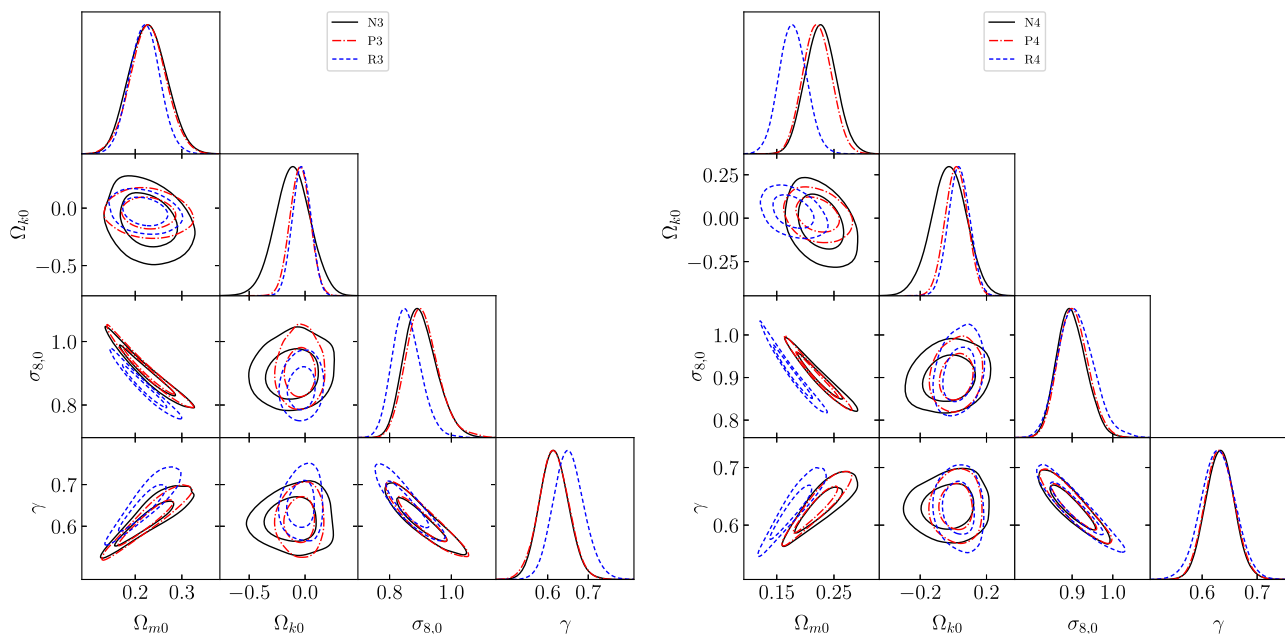


FIG. 6. Contour plots and the marginalized likelihood of  $H_0$  and  $\Omega_{k0}$  considering the Matérn 9/2 covariance for Set III (left) and Set IV (right). The solid lines represent the results for N3 and N4 dataset combination, dash-dot lines corresponds to the P3 and P4 dataset combination, and the dashed lines represent the results for R3 and R4 dataset combinations. The associated  $1\sigma$ ,  $2\sigma$  confidence contours are shown along with the respective marginalized likelihood functions.

the analysis results in tighter constraints on  $\Omega_{k0}$ . Combining the CC and Pantheon data with the BAO data, it can be seen that  $\Omega_{k0}$  is consistent with a spatially flat universe at the  $1\sigma$  CL for the squared exponential, Matérn 9/2 and Cauchy covariance, whereas in  $2\sigma$  for the rational

quadratic kernel. The best-fit values show an inclination toward a closed universe in these cases. This result is obtained without using any given  $H_0$  priors. We then introduce the P18 and R19  $H_0$  measurements as priors in our analysis and examine their effect on the reconstruction.

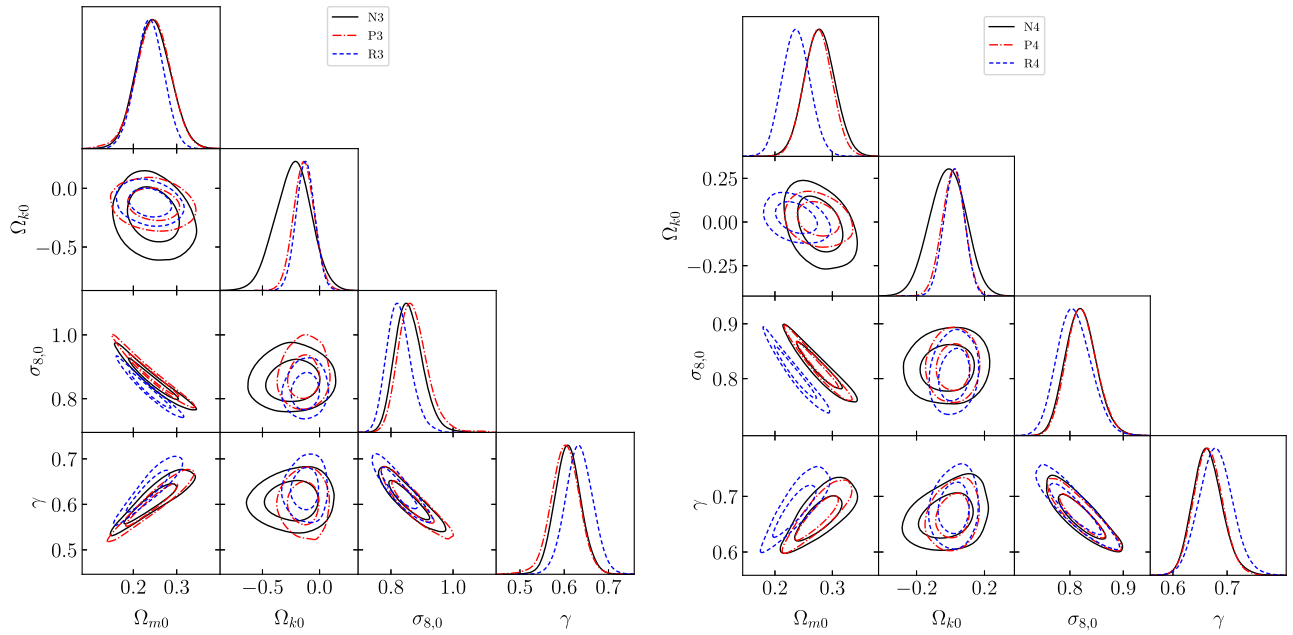


FIG. 7. Contour plots and the marginalized likelihood of  $H_0$  and  $\Omega_{k0}$  considering the Cauchy covariance for Set III (left) and Set IV (right). The solid lines represent the results for N3 and N4 dataset combination, dash-dot lines corresponds to the P3 and P4 dataset combination, and the dashed lines represent the results for R3 and R4 dataset combinations. The associated  $1\sigma$ ,  $2\sigma$  confidence contours are shown along with the respective marginalized likelihood functions.

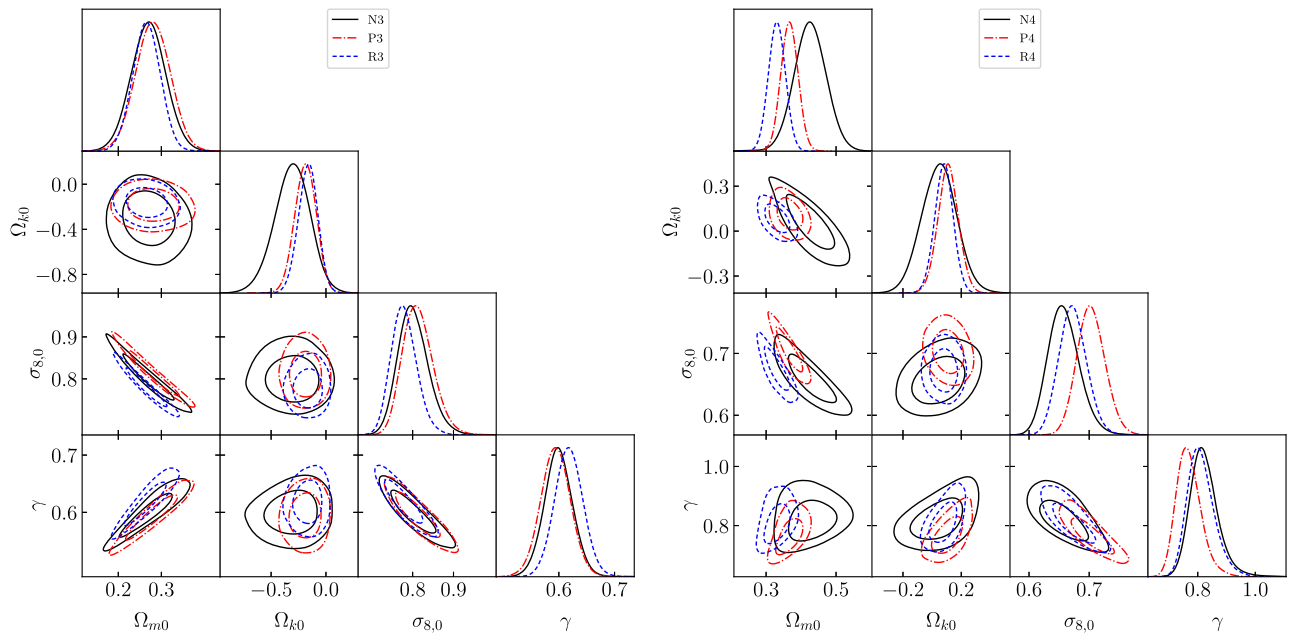


FIG. 8. Contour plots and the marginalized likelihood of  $H_0$  and  $\Omega_{k0}$  considering the rational quadratic covariance for Set III (left) and Set IV (right). The solid lines represent the results for N3 and N4 dataset combination, dash-dot lines corresponds to the P3 and P4 dataset combination, and the dashed lines represent the results for R3 and R4 dataset combinations. The associated  $1\sigma$ ,  $2\sigma$  confidence contours are shown along with the respective marginalized likelihood functions.

Plots reveal that the best-fit values of  $\Omega_{k0}$  favor a spatially open universe for the P18 prior choice, whereas the R19 prior favors a spatially closed universe, except for the squared exponential kernel which favors a spatially open universe for both the P18 and R19 priors. However, a

spatially flat universe is mostly included at  $2\sigma$  CL for both cases (see Table I).

Consistency with thermodynamic requirements imposed by the generalized second law of thermodynamics for the reconstructed constraints on  $\Omega_{k0}$  from the background data



combinations are checked quite exhaustively. This has been done with the help of the inequality very recently given by Ferreira and Pavón [35] (see also Ref. [132]). It is quite encouraging to see that the constraints obtained are quite consistent with the thermodynamic requirements, independent of the choice of the kernel for all possible combinations of datasets (see Table I).

In addition to the background data, we also utilize the RSD data to determine  $\Omega_{k0}$  using two combination of datasets, CC + Pantheon + RSD and CC +  $r$ BAO + Pantheon + RSD respectively. This inclusion does not help in providing tighter constraints on  $\Omega_{k0}$ , but is essential as the spatial curvature and the formation of large scale structure should be compatible. We also include the R18 and P18  $H_0$  priors and see their effect on the reconstruction. The results obtained are consistent with spatial flatness mostly within  $2\sigma$  and always within  $3\sigma$  in the domain of the reconstruction,  $0 < z < 2$  (see Table II).

The GP method has previously been used for constraining  $\Omega_{k0}$  from observations. Li *et al.* [21] constrained the spatial curvature to be  $\Omega_{k0} = -0.045^{+0.172}_{-0.172}$  with  $22H(z)$  and Union 2.1 SN-Ia data, and  $\Omega_{k0} = -0.140^{+0.161}_{-0.158}$  considering the JLA SN-Ia data, which are in good agreement with a spatially flat universe. Wei and Wu [22] extended this analysis using different  $H_0$  priors and showed that the local and global  $H_0$  measurements can affect the constraints on  $\Omega_{k0}$ . Wang *et al.* [25] showed that a spatially flat and transparent universe is preferred by observations. The results indicated a strong degeneracy between the curvature parameter and cosmic opacity. From 100 simulated GWs signals, Liao [26] found the results favored a spatially flat universe with 0.057 uncertainty at  $1\sigma$ , which was reduced to 0.027 for 1000 GWs signals. On combining with the SN-Ia data from DES, the uncertainty was further constrained to 0.027 and 0.018 respectively. The analysis by Wei and Melia [27] suggests that a mildly closed universe ( $\Omega_{k0} = -0.918 \pm 0.429$ ) is preferred at the  $1\sigma$  level using quasars and CC data. Recently, Wang *et al.* [32] found a spatially open universe is favored at  $1\sigma$  CL using 31 CC-H(z) measurements and simulated data from GWs, based on the ANN method. Another nonparametric reconstruction of  $\Omega_{k0}$  utilizing different approaches like the principal component analysis, genetic algorithms, binning with direct

error propagation and the Padé approximation, was carried out by Sapone *et al.* [20]. Their results were in good agreement with  $\Omega_k = 0$  at the  $1\sigma$  CL.

Our work is similar to the recent works by Yang and Gong [33] and Dhawan *et al.* [34], but there are quite a few differences to list. Yang and Gong [33], Dhawan *et al.* [34] have used the Pantheon compilation by Scolnic *et al.* [31] in their analysis. However, in this work we have utilized the very recent redshift corrected version of Pantheon compilation by Steinhardt *et al.* [68]. Yang and Gong [33] reconstructed the quantity  $\Omega_{k0}h^2$  so that the discrepancy in the present value of Hubble parameter  $H_0$  is avoided. Dhawan *et al.* [34] obtained constraints on  $\Omega_{k0}$  independent of the absolute calibration of either the SN-Ia or CC measurements. In this particular work, we have obtained constraints on both  $\Omega_{k0}$  and  $H_0$  from the combined CC + Pantheon data, thereby capturing the degeneracy or correlation between them. Yang and Gong [33] imposed a zero mean function, which follows the work Seikel *et al.* [40] and is similar to our work. Dhawan *et al.* [34], on the other hand used a mean nonzero constant prior equal to 100, following Shafieloo *et al.* [41]. Utilizing solely the background data, Yang and Gong [33] found the case for a spatially open universe from the combined CC and Pantheon data at more than  $1\sigma$  CL considering the squared exponential covariance. The present work starts with a zero mean prior similar to [33], but the best-fit value for the combined CC + Pantheon data (N1) using the same squared exponential kernel favors a spatially closed universe, and  $\Omega_{k0} = 0$  is well included within  $1\sigma$  CL. This result is similar in nature to that given by Dhawan *et al.* [34] where the obtained constraints on  $\Omega_{k0} = -0.03 \pm 0.26$  are consistent with spatial flatness at the  $\mathcal{O}(10^{-1})$  level. The qualitative difference of the present result with that obtained in [33] can stem from the fact that we have used the redshift corrected version of the Pantheon compilation [68].

Our conclusion is that although there is indeed a scope of revisiting the notion of a spatially flat universe, but the present state of affairs is still quite consistent with  $k = 0$ . Observations from future surveys, as well as more data on high redshift observations of CC, SN, BAO, and other observables should be able to provide tighter constraints on  $\Omega_{k0}$ .

- 
- [1] A. R. Liddle and D. H. Lyth, *Cosmological Inflation and Large Scale Structure* (Cambridge University Press, Cambridge, England, 2000).  
 [2] C. Clarkson, M. Cortes, and B. A. Bassett, *J. Cosmol. Astropart. Phys.* **08** (2007) 011.  
 [3] Y.-G. Gong and A. Wang, *Phys. Rev. D* **75**, 043520 (2007).

- [4] N. Aghanim *et al.* (Planck Collaboration), *Astron. Astrophys.* **641**, A6 (2020).  
 [5] C. D. Leonard, P. Bull, and R. Allison, *Phys. Rev. D* **94**, 023502 (2016).  
 [6] A. Witzemann, P. Bull, C. Clarkson, M. G. Santos, M. Spinelli, and A. Weltman, *Mon. Not. R. Astron. Soc.* **477**, L122 (2018).



- [7] M. Denissenya, E. V. Linder, and A. Shafieloo, *J. Cosmol. Astropart. Phys.* **03** (2018) 041.
- [8] S. Cao, J. Qi, M. Biesiada, X. Zheng, T. Xu, Y. Pan, and Z.-H. Zhu, *Phys. Dark Universe* **24**, 100274 (2019).
- [9] E.-K. Li, M. Du, and L. Xu, *Mon. Not. R. Astron. Soc.* **491**, 4960 (2020).
- [10] G. Efstathiou and S. Gratton, *Mon. Not. R. Astron. Soc.* **496**, L91 (2020).
- [11] C.-G. Park and B. Ratra, *Phys. Rev. D* **101**, 083508 (2020).
- [12] R. C. Nunes and A. Bernui, *Eur. Phys. J. C* **80**, 1025 (2020).
- [13] D. Benisty and D. Staicova, *Astron. Astrophys.* **647**, A38 (2021).
- [14] W. Handley, *Phys. Rev. D* **103**, 063529 (2021).
- [15] C. Clarkson, B. Bassett, and T. H.-C. Lu, *Phys. Rev. Lett.* **101**, 011301 (2008).
- [16] R.-G. Cai, Z.-K. Guo, and T. Yang, *Phys. Rev. D* **93**, 043517 (2016).
- [17] A. Rana, D. Jain, S. Mahajan, and A. Mukherjee, *J. Cosmol. Astropart. Phys.* **03** (2017) 028.
- [18] Y. Liu, S. Cao, T. Liu, X. Li, S. Geng, Y. Lian, and W. Guo, *Astrophys. J.* **901**, 129 (2020).
- [19] R. Arjona and S. Nesseris, *Phys. Rev. D* **103**, 103539 (2021).
- [20] D. Sapone, E. Majerotto, and S. Nesseris, *Phys. Rev. D* **90**, 023012 (2014).
- [21] Z. Li, G.-J. Wang, K. Liao, and Z.-H. Zhu, *Astrophys. J.* **833**, 240 (2016).
- [22] J.-J. Wei and X.-F. Wu, *Astrophys. J.* **838**, 160 (2017).
- [23] N. Suzuki, D. Rubin, C. Lidman *et al.*, *Astrophys. J.* **746**, 85 (2012).
- [24] M. Betoule *et al.* (SDSS Collaboration), *Astron. Astrophys.* **568**, A22 (2014).
- [25] G.-J. Wang, J.-J. Wei, Z.-X. Li, J.-Q. Xia, and Z.-H. Zhu, *Astrophys. J.* **847**, 45 (2017).
- [26] K. Liao, *Phys. Rev. D* **99**, 083514 (2019).
- [27] J.-J. Wei and F. Melia, *Astrophys. J.* **888**, 99 (2020).
- [28] C.-Z. Ruan, F. Melia, Y. Chen, and T.-J. Zhang, *Astrophys. J.* **881**, 137 (2019).
- [29] H. Zhou and Z. Li, *Astrophys. J.* **889**, 186 (2020).
- [30] B. Wang, J.-Z. Qi, J.-F. Zhang, and X. Zhang, *Astrophys. J.* **898**, 100 (2020).
- [31] D. M. Scolnic *et al.*, *Astrophys. J.* **859**, 101 (2018).
- [32] G.-J. Wang, X.-J. Ma, and J.-Q. Xia, *Mon. Not. R. Astron. Soc.* **501**, 5714 (2021).
- [33] Y. Yang and Y. Gong, *Mon. Not. R. Astron. Soc.* **504**, 3092 (2021).
- [34] S. Dhawan, J. Alsing, and S. Vagnozzi, *Mon. Not. R. Astron. Soc.* **506**, L1 (2021).
- [35] P. C. Ferreira and D. Pavón, *Universe* **2**, 27 (2016).
- [36] C. Williams, *Prediction with Gaussian Processes: From Linear Regression to Linear Prediction and Beyond, Learning in Graphical Models*, edited by M. I. Jordan (MIT Press, Cambridge, Massachusetts, 1999).
- [37] D. MacKay, *Information Theory, Inference and Learning Algorithms* (Cambridge University Press, Cambridge, England, 2003).
- [38] C. Rasmussen and C. Williams, *Gaussian Processes for Machine Learning* (MIT Press, Cambridge, Massachusetts, 2006).
- [39] T. Holsclaw, U. Alam, B. Sansó, H. Lee, K. Heitmann, S. Habib, and D. Higdon, *Phys. Rev. Lett.* **105**, 241302 (2010).
- [40] M. Seikel, C. Clarkson, and M. Smith, *J. Cosmol. Astropart. Phys.* **06** (2012) 036.
- [41] A. Shafieloo, A. G. Kim, and E. V. Linder, *Phys. Rev. D* **85**, 123530 (2012).
- [42] S. Yahya, M. Seikel, C. Clarkson, R. Maartens, and M. Smith, *Phys. Rev. D* **89**, 023503 (2014).
- [43] S. Santos-da Costa, V. C. Busti, and R. F. Holanda, *J. Cosmol. Astropart. Phys.* **10** (2015) 061.
- [44] T. Yang, Z.-K. Guo, and R.-G. Cai, *Phys. Rev. D* **91**, 123533 (2015).
- [45] R.-G. Cai, Z.-K. Guo, and T. Yang, *Phys. Rev. D* **93**, 043517 (2016).
- [46] D. Wang and X.-H. Meng, *Phys. Rev. D* **95**, 023508 (2017).
- [47] D. Wang, W. Zhang, and X.-H. Meng, *Eur. Phys. J. C* **79**, 211 (2019).
- [48] L. Zhou, X. Fu, Z. Peng, and J. Chen, *Phys. Rev. D* **100**, 123539 (2019).
- [49] Y.-F. Cai, M. Khurshudyan, and E. N. Saridakis, *Astrophys. J.* **888**, 62 (2020).
- [50] P. Mukherjee and N. Banerjee, [arXiv:2007.15941](https://arxiv.org/abs/2007.15941).
- [51] H.-N. Lin, X. Li, and L. Tang, *Chin. Phys. C* **43**, 075101 (2019).
- [52] M.-J. Zhang and J.-Q. Xia, *J. Cosmol. Astropart. Phys.* **12** (2016) 005.
- [53] J. F. Jesus, R. Valentim, A. A. Escobal, and S. H. Pereira, *J. Cosmol. Astropart. Phys.* **04** (2020) 053.
- [54] R. E. Keeley, A. Shafieloo, G.-B. Zhao, J. Alberto Vazquez, and H. Koo, *Astron. J.* **161**, 151 (2021).
- [55] P. Mukherjee and A. Mukherjee, *Mon. Not. R. Astron. Soc.* **504**, 3938 (2021).
- [56] P. Mukherjee and N. Banerjee, *Eur. Phys. J. C* **81**, 36 (2021).
- [57] P. Mukherjee and N. Banerjee, *Phys. Rev. D* **103**, 123530 (2021).
- [58] D. Benisty, *Phys. Dark Universe* **31**, 100766 (2021).
- [59] K. Bora and S. Desai, *J. Cosmol. Astropart. Phys.* **06** (2021) 052.
- [60] R. Jimenez and A. Loeb, *Astrophys. J.* **573**, 37 (2002).
- [61] J. Simon, L. Verde, and R. Jimenez, *Phys. Rev. D* **71**, 123001 (2005).
- [62] C. Zhang, H. Zhang, S. Yuan, T.-J. Zhang, and Y.-C. Sun, *Res. Astron. Astrophys.* **14**, 1221 (2014).
- [63] D. Stern, R. Jimenez, L. Verde, M. Kamionkowski, and S. A. Stanford, *J. Cosmol. Astropart. Phys.* **02** (2010) 008.
- [64] M. Moresco, A. Cimatti, R. Jimenez, and L. Pozzetti, *J. Cosmol. Astropart. Phys.* **08** (2012) 006.
- [65] M. Moresco, *Mon. Not. R. Astron. Soc.* **450**, L16 (2015).
- [66] M. Moresco, L. Pozzetti, A. Cimatti, R. Jimenez, C. Maraston, L. Verde, D. Thomas, A. Citro, R. Tojeiro, and D. Wilkinson, *J. Cosmol. Astropart. Phys.* **05** (2016) 014.
- [67] A. L. Ratsimbazafy, S. I. Loubser, S. M. Crawford, C. M. Cress, B. A. Bassett, R. C. Nichol, and P. Väisänen, *Mon. Not. R. Astron. Soc.* **467**, 3239 (2017).
- [68] C. L. Steinhardt, A. Sneppen, and B. Sen, *Astrophys. J.* **902**, 14 (2020).

- [69] E. Gaztanaga, A. Cabre, and L. Hui, *Mon. Not. R. Astron. Soc.* **399**, 1663 (2009).
- [70] A. Oka, S. Saito, T. Nishimichi, A. Taruya, and K. Yamamoto, *Mon. Not. R. Astron. Soc.* **439**, 2515 (2014).
- [71] Y. Wang *et al.* (BOSS Collaboration), *Mon. Not. R. Astron. Soc.* **469**, 3762 (2017).
- [72] C.-H. Chuang and Y. Wang, *Mon. Not. R. Astron. Soc.* **435**, 255 (2013).
- [73] S. Alam *et al.* (BOSS Collaboration), *Mon. Not. R. Astron. Soc.* **470**, 2617 (2017).
- [74] C. Blake *et al.*, *Mon. Not. R. Astron. Soc.* **425**, 405 (2012).
- [75] C.-H. Chuang *et al.*, *Mon. Not. R. Astron. Soc.* **433**, 3559 (2013).
- [76] L. Anderson *et al.* (BOSS Collaboration), *Mon. Not. R. Astron. Soc.* **441**, 24 (2014).
- [77] G.-B. Zhao *et al.*, *Mon. Not. R. Astron. Soc.* **482**, 3497 (2019).
- [78] N. G. Busca, T. Delubac, J. Rich *et al.*, *Astron. Astrophys.* **552**, A96 (2013).
- [79] J. E. Bautista *et al.*, *Astron. Astrophys.* **603**, A12 (2017).
- [80] T. Delubac *et al.* (BOSS Collaboration), *Astron. Astrophys.* **574**, A59 (2015).
- [81] A. Font-Ribera *et al.* (BOSS Collaboration), *J. Cosmol. Astropart. Phys.* **05** (2014) 027.
- [82] E.-K. Li, M. Du, Z.-H. Zhou, H. Zhang, and L. Xu, *Mon. Not. R. Astron. Soc.* **501**, 4452 (2021).
- [83] A. G. Riess, S. Casertano, W. Yuan, L. M. Macri, and D. Scolnic, *Astrophys. J.* **876**, 85 (2019).
- [84] C. Blake *et al.*, *Mon. Not. R. Astron. Soc.* **425**, 405 (2012).
- [85] D. H. Jones *et al.*, *Mon. Not. R. Astron. Soc.* **355**, 747 (2004).
- [86] S. Alam *et al.* (SDSS-III Collaboration), *Astrophys. J. Suppl. Ser.* **219**, 12 (2015).
- [87] Y. Wang, G.-B. Zhao, C.-H. Chuang, M. Pellejero-Ibanez, C. Zhao, F.-S. Kitaura, and S. Rodriguez-Torres, *Mon. Not. R. Astron. Soc.* **481**, 3160 (2018).
- [88] L. Guzzo *et al.*, *Astron. Astrophys.* **566**, A108 (2014).
- [89] A. de Mattia *et al.*, *Mon. Not. R. Astron. Soc.* **501**, 5616 (2021).
- [90] A. Tamone *et al.*, *Mon. Not. R. Astron. Soc.* **499**, 5527 (2020).
- [91] M. Aubert *et al.*, arXiv:2007.09013.
- [92] G.-B. Zhao *et al.*, *Mon. Not. R. Astron. Soc.* **504**, 33 (2021).
- [93] H. Gil-Marín *et al.*, *Mon. Not. R. Astron. Soc.* **498**, 2492 (2020).
- [94] R. Neveux *et al.*, *Mon. Not. R. Astron. Soc.* **499**, 210 (2020).
- [95] J. E. Bautista *et al.*, *Mon. Not. R. Astron. Soc.* **500**, 736 (2020).
- [96] K. Said, M. Colless, C. Magoulas, J. R. Lucey, and M. J. Hudson, *Mon. Not. R. Astron. Soc.* **497**, 1275 (2020).
- [97] F. Qin, C. Howlett, and L. Staveley-Smith, *Mon. Not. R. Astron. Soc.* **487**, 5235 (2019).
- [98] C. Blake, P. Carter, and J. Koda, *Mon. Not. R. Astron. Soc.* **479**, 5168 (2018).
- [99] P. Zarrouk *et al.*, *Mon. Not. R. Astron. Soc.* **477**, 1639 (2018).
- [100] G.-B. Zhao *et al.*, *Mon. Not. R. Astron. Soc.* **482**, 3497 (2019).
- [101] R. Ruggeri *et al.*, *Mon. Not. R. Astron. Soc.* **483**, 3878 (2019).
- [102] C. Adams and C. Blake, *Mon. Not. R. Astron. Soc.* **471**, 839 (2017).
- [103] Z. Li, Y. Jing, P. Zhang, and D. Cheng, *Astrophys. J.* **833**, 287 (2016).
- [104] C.-H. Chuang *et al.* (BOSS Collaboration), *Mon. Not. R. Astron. Soc.* **471**, 2370 (2017).
- [105] A. G. Sanchez *et al.* (BOSS Collaboration), *Mon. Not. R. Astron. Soc.* **464**, 1640 (2017).
- [106] F. A. Marn, F. Beutler, C. Blake, J. Koda, E. Kazin, and D. P. Schneider, *Mon. Not. R. Astron. Soc.* **455**, 4046 (2016).
- [107] Y. Wang, *Mon. Not. R. Astron. Soc.* **443**, 2950 (2014).
- [108] S. Satpathy *et al.* (BOSS Collaboration), *Mon. Not. R. Astron. Soc.* **469**, 1369 (2017).
- [109] T. Okumura *et al.*, *Publ. Astron. Soc. Jpn.* **68**, 38 (2016).
- [110] R. Holanda, J. Carvalho, and J. Alcaniz, *J. Cosmol. Astropart. Phys.* **04** (2013) 027.
- [111] R. Kessler and D. Scolnic, *Astrophys. J.* **836**, 56 (2017).
- [112] D. Foreman-Mackey, D. W. Hogg, D. Lang, and J. Goodman, *Publ. Astron. Soc. Pac.* **125**, 306 (2013).
- [113] A. Lewis, arXiv:1910.13970.
- [114] G. W. Gibbons and S. W. Hawking, *Phys. Rev. D* **15**, 2738 (1977).
- [115] T. Jacobson, *Phys. Rev. Lett.* **75**, 1260 (1995).
- [116] T. Padmanabhan, *Phys. Rep.* **380**, 235 (2003).
- [117] D. Bak and S. J. Rey, *Classical Quantum Gravity* **17**, L83 (2000).
- [118] S. Frautschi, *Science* **217**, 593 (1982).
- [119] D. Polarski, A. A. Starobinsky, and H. Giacomini, *J. Cosmol. Astropart. Phys.* **12** (2016) 037.
- [120] L. Xu, *Phys. Rev. D* **88**, 084032 (2013).
- [121] J. R.-Zapatero, C. García-García, D. Alonso, P. G. Ferreira, and R. D. P. Grumitt, arXiv:2201.07025.
- [122] Y. Gong, M. Ishak, and A. Wang, *Phys. Rev. D* **80**, 023002 (2009).
- [123] L.-M. Wang and P. J. Steinhardt, *Astrophys. J.* **508**, 483 (1998).
- [124] E. V. Linder, *Phys. Rev. D* **72**, 043529 (2005).
- [125] E. V. Linder and R. N. Cahn, *Astropart. Phys.* **28**, 481 (2007).
- [126] H. Wei, *Phys. Lett. B* **664**, 1 (2008).
- [127] Q. Gao and Y. Gong, *Classical Quantum Gravity* **31**, 105007 (2014).
- [128] R. A. Battye, T. Charnock, and A. Moss, *Phys. Rev. D* **91**, 103508 (2015).
- [129] P. Bull *et al.*, *Phys. Dark Universe* **12**, 56 (2016).
- [130] J. Sol Peracaula, J. d. C. Perez, and A. Gomez-Valent, *Mon. Not. R. Astron. Soc.* **478**, 4357 (2018).
- [131] I. G. McCarthy, S. Bird, J. Schaye, J. Harnois-Deraps, A. S. Font, and L. Van Waerbeke, *Mon. Not. R. Astron. Soc.* **476**, 2999 (2018).
- [132] J. P. Mimoso and D. Pavón, *Phys. Rev. D* **94**, 103507 (2016).